Influence of Oxygen Vibrational Excitation on HS + O−2 Reactive Collisions

ARTICLE *in* INTERNATIONAL JOURNAL OF QUANTUM CHEMISTRY · MARCH 2010

Impact Factor: 1.43 · DOI: 10.1002/qua.22135

3 AUTHORS:

Juan D Garrido
Universidade Federal da Integração Latino-…
13 PUBLICATIONS **87** CITATIONS
SEE PROFILE

Marco Nascimento
Federal University of Rio de Janeiro
143 PUBLICATIONS **1,914** CITATIONS
SEE PROFILE

Maikel Y Ballester
Federal University of Juiz de Fora
17 PUBLICATIONS **72** CITATIONS
SEE PROFILE

Influence of Oxygen Vibrational Excitation on HS + O_2 Reactive Collisions

JUAN DE DIOS GARRIDO,[1] MARCO ANTONIO CHAER NASCIMENTO,[2] MAIKEL YUSAT BALLESTER[3]

[1]*Departamento de Ciencias Básicas, Instituto Tecnológico de Pachuca, México*
[2]*Departamento de Físico-Química, Instituto de Química, Universidade Federal do Rio de Janeiro*
[3]*Grupo de Modelacion, Centro de Estudios Ambientales de Cienfuegos, Cuba*

Received 2 December 2008; accepted 21 January 2009
Published online 23 June 2009 in Wiley InterScience (www.interscience.wiley.com).
DOI 10.1002/qua.22135

ABSTRACT: The title reaction is studied in the frame of quasiclassical trajectory method using a previously reported global potential energy surface for the ground electronic state of HSO_2. To assert the role of vibrational excitation in molecular oxygen, specific calculations at some vibrational quantum states were carried out. To take into account the zero point energy leakage of the classical calculations, a passive method, Internal Energy Quantum Mechanical Threshold is used. HSO + O are the most formed set of products. Total reactive cross-sections are calculated and fitted to models in the studied energy range. Analytical expression for rate coefficients are reported as well. A comparison of reactivities when vibrational energy is deposited either in O_2 or in HS is also presented.

Key words: molecular dynamics; sulfur

1. Introduction

Vibrationally excited molecular species in the atmosphere are produced both by chemical reactions and by the interaction of molecules with electromagnetic radiation. Particularly at stratosphere and mesosphere where pressure is relatively low, relaxation processes through molecular collisions are more likely to be slow [1–10]; hence, the internal energy content of the constituents of such layers is expected to be far from thermal equilibrium.

In a previous work [11], the title reaction was studied. Reactants rovibrational states were there fixed at the ground level but some vibrational excited levels of the mercapto radical (HS) were also studied. It was shown that the HS vibrational energy plays a significant role when comparing theoretical rate constants values with the available experimental data.

Correspondence to: M. Y. Ballester; e-mail: maikel.ballester@gmail.com
M. Y. Ballester is currently at Universidade Federal de Juiz de Fora, Brasil.
Contract grant sponsor: Third World Academy of Science (TWAS).
Contract grant number: 97-144, RG/CHE/LA.
Contract grant sponsor: German Academic Exchange Service (DAAD).
Contract grant sponsor: Fundação de Amparo à Pesquisa do Estado de Minas Gerais (FAPEMIG), Brasil.
Contract grant number: CEX 00265/08.

Vibrationally excited molecular oxygen is formed in the atmosphere from ozone photolysis at several wave lengths [7, 9, 12–15] and also from different atmospheric reactions [16, 17]. Such species can react with HS radicals produced or ejected from strong volcanic eruptions in different layers of the atmosphere. Therefore, a complete description of the reaction between the mercapto radical with molecular oxygen requires to account for the internal states of the reactants. Thus, this work is aimed at studying the role of vibrational excitation energy of molecular oxygen in the reaction:

$$HS(v' = 0, j' = 1) + O_2(v'', j'' = 1) \rightarrow \text{products} \quad (1)$$

using the quasiclassical trajectory method and a global potential energy surface for the ground electronic state of HSO_2, previously reported by one of us [18]. This methodology has already been used in previous studies concerning the HSO_2 molecular system [11, 19–21] furnishing good results when compared with the experimental data and new insights for the studied processes.

This article is organized as follows: the main features of the potential energy surface are presented in Section 2. Section 3 provides details of the calculation methods. Results are gathered and discussed in Section 4 followed by the conclusions.

2. Potential Energy Surface

All the calculations reported in this work were carried out employing a six-dimensional potential energy surface (PES) for HSO_2 developed previously [18]. This PES, describing the interaction energy for any configuration of such a tetratomic system, was constructed according to the Double Many-Body Expansion method (DMBE, see references therein Ref. 18). It uses two- and three-body DMBE functions for the corresponding fragments and additional four-body energy terms accounting for electrostatic four-body interactions and short range terms, calibrated to properly mimic ab initio calculations at CASPT2/FVCAS/AVXZ ($X = 2, 3$) level. For further details about the surface the reader is referred to the original article [18].

For the interest of this work we represent in Figure 1 the energetic profile of the PES. The solid or dashed lines in Figure 1 connect the reagents and products to the respective transition states. Energies

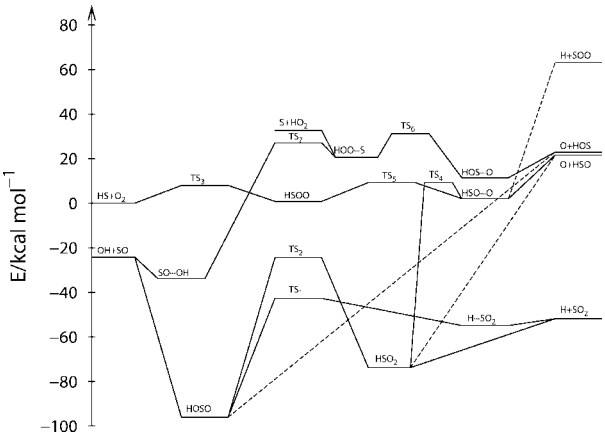

FIGURE 1. Energetic diagram of the potential energy surface for HSO_2 used in this work. Solid and dashed lines represent minimum energy path between the different conformers, TS_n denotes transition states. Zero point energies were not included in the diagram.

in Figure 1 do not include zero point energy values. The notation is the same used in previous articles [11, 18]. Notice that the direct pathway, represented with a dashed line, between the HSO_2 and HSO + O was already discussed elsewhere [22].

3. Computational Procedures

All calculations in this work have employed the quasiclassical trajectory (QCT) method as implemented in the MERCURY/VENUS96 [23] code, which has been suitably modified to accommodate the HSO_2 DMBE potential energy surface. For the numerical integrations, a step size of 2.5×10^{-16} s has been used, warranting a total energy conservation better than two parts in 10^5. The procedure employed to assign the various reactive channels has been described elsewhere [24]. As for the OH + SO reaction [19], there are 14 exit channels because we do not consider as distinct those corresponding to isomers of a given species.

Calculations were carried out at specific rovibrational reactants states for diatom–diatom translational energies in the range $1 \leq E_{tr}(\text{kcal/mol}) \leq 40$. However, we have done calculations in the range from small to middle translational energies, which are likely to be of major interest for atmospheric chemistry. Yet, since the sets of calculations for low translational energies are computationally expensive, we have limited their number to a minimum

considered adequate for a satisfactory coverage. For comparison with previous calculations [11], the initial rotational quantum number of the colliding molecules has been fixed at their ground state level. To select the maximum value of the impact parameter (b_{max}) leading to reaction, the usual procedure has been used, computing sets of 300 trajectories for fixed values of b to obtain an accuracy in b_{max} of about ± 0.1 Å. In all cases, diatomic–diatomic initial separation has been fixed at 10 Å, to make the interaction negligible. To yield reactive cross-sections with an error of typically a few percent, sets of 5,000 trajectories have been run for each translational energy and ro-vibrational combination, making a total of about 2.65×10^5 trajectories.

For a given translational energy, the reactive cross-section has been calculated by using $\sigma_r = \pi b_{max}^2 P_r$, with the associated 68% uncertainties being [25] $\Delta\sigma_r = \sigma_r[(N_T - N_r)/(N_T N_r)]^{1/2}$; N_r is the number of reactive trajectories in a total of N_T, and $P_r = N_r/N_T$ the reaction probability. From the reactive cross-section and assuming a Maxwell-Boltzmann distribution over the translational energy, the specific thermal rate coefficient assumes the form:

$$k(T) = g_e(T)\left(\frac{2}{k_B T}\right)^{3/2}\left(\frac{1}{\pi\mu}\right)^{1/2} \int_0^\infty E_{tr}\sigma(E_{tr})\exp(-E_{tr}/k_B T)dE_{tr} \quad (2)$$

where T is the temperature, k_B the Boltzmann constant, μ the reactants reduced mass, and $g_e = \frac{1}{3}[1 + \exp(-544.7/T)]^{-1}$ is the corresponding electronic degeneracy factor [11, 26, 27].

4. Results and Discussion

4.1. REACTIVE CHANNELS

Tables I and II summarize the trajectory calculations carried out in the present work for the title ($HS(v' = 0, j' = 1) + O_2(v'', j'' = 1)$) reaction. Column one of these tables indicates the vibrational quantum number of the O_2 molecule (v''), whereas the studied translational energies are given in column two. In this article, we focused in the loss of HS radical, and therefore the last four columns of the tables show values of the total reactive cross-section and its associated uncertainties, without specifying which product was formed during the reactive collision.

To account for the well-known zero-point energy (ZPE) leakage of the classical calculations, we have used the nonactive internal energy quantum mechanical threshold (IEQMT) method [28] to compare with the pure QCT results. Following this method, only those trajectories for which the internal energy of each product exceeds its ZPE have been included in the statistical analysis. The fourth and fifth columns of Tables I and II show total and reactive trajectories according to the IEQMT criteria, whereas the sixth column presents the reactive trajectories according the QCT calculations. From Tables I and II, IEQMT cross-sections shows up the same qualitative behavior as QCT. The obtained reactivity accounting ZPE is in general slightly larger than the corresponding for pure QCT.

As indicated before [11], and according to the energetic of the potential energy surface represented in Figure 1, all reactive channels are closed for low translational energies when reactants are at their ground vibrational levels. For vibrational excitation energy values in the O_2 molecule up to 47.59 kcal/mol (corresponding to vibrational quantum number $v'' = 11$) the reactive channels remain closed for translational energies below a given threshold value (E_{tr}^{th}). For larger vibrational excitation energies such a threshold disappears and the reactive channels are open over the whole range of translational energies considered in the present work. In a previous article [11], we have shown that for some combination of vibration and translational energies, SO_2 was the dominant product. Differently, in the present case, HSO is the dominant product for all the investigated combinations of vibration and translational energies. Even though HSO and SO_2 are the major products of reaction (1), other reactive channels are also opened (an example is included in Table III). A detailed analysis of all reactive channels is out of the scope of this work and it will be hopefully reported in a forthcoming paper.

In this work, the total energies used are, in general, quite above the energy of transition states TS_3 and TS_5 in Figure 1. This implies that the QCT technique is ideally suited for the present study as the number of accessible states is large.

4.2. REACTIVE CROSS-SECTIONS

We now examine the shape of the excitation functions (cross section vs. translational energy) for any product formation, displayed in Figure 2 together with the associated error bars. As we have pointed

TABLE I

Trajectory calculations results for the reaction $HS(0,1) + O_2(v'',1)$.

v''	E_{tr} (Kcal/mol)	b_{max} (Å)	N_T^{IEQMT}	N_r^{IEQMT}	N_r^{QCT}	σ^r_{IEQMT}	$\Delta\sigma^r_{IEQMT}$	σ^r_{QCT}	$\Delta\sigma^r_{QCT}$
0	20.0	0.6	3,774	54	54	0.016	0.002	0.012	0.002
	22.5	1.3	4,075	23	25	0.030	0.006	0.027	0.005
	24.0	1.3	3,980	38	46	0.051	0.008	0.049	0.007
	28.0	1.5	4,013	73	78	0.129	0.015	0.110	0.012
	32.0	1.6	4,168	109	111	0.210	0.020	0.179	0.017
	36.0	1.7	4,061	201	204	0.450	0.030	0.370	0.025
	40.0	1.8	4,165	310	310	0.758	0.041	0.631	0.035
	45.0	1.8	4,221	547	547	1.319	0.053	1.114	0.044
5	15.0	1.4	4,533	14	14	0.019	0.005	0.017	0.005
	17.5	1.6	4,532	111	113	0.197	0.018	0.182	0.017
	20.0	1.9	4,525	250	250	0.627	0.038	0.567	0.035
	25.0	2.0	4,585	550	550	1.507	0.060	1.382	0.056
	30.0	2.2	4,593	732	735	2.423	0.082	2.235	0.076
	35.0	2.3	4,629	920	926	3.303	0.097	3.078	0.091
	40.0	2.3	4,671	1,069	1,075	3.803	0.102	3.573	0.097
	45.0	2.4	4,673	1,182	1,182	4.577	0.115	4.278	0.109
9	12.5	1.7	4,394	72	72	0.149	0.017	0.131	0.015
	15.0	2.2	4,485	197	197	0.669	0.046	0.599	0.042
	17.5	2.1	4,491	422	425	1.302	0.060	1.178	0.055
	20.0	2.2	4,559	585	588	1.951	0.075	1.788	0.069
	22.5	2.4	4,643	673	673	2.623	0.094	2.436	0.087
	25.0	2.4	4,630	865	865	3.381	0.104	3.131	0.097
	35.0	2.6	4,665	1,253	1,258	5.274	0.127	5.476	0.120
	40.0	2.5	4,713	1,537	1,537	6.403	0.134	6.036	0.128
	45.0	2.5	4,746	1,619	1,622	6.698	0.135	6.370	0.130
12	1.0	4.1	3,841	194	194	2.667	0.187	2.049	0.144
	2.5	3.3	4,214	224	224	1.819	0.118	1.533	0.100
	7.5	2.7	4,415	130	134	0.674	0.058	0.614	0.052
	10.0	2.7	4,458	168	168	0.863	0.065	0.770	0.058
	15.0	2.8	4,518	429	431	2.339	0.107	2.123	0.098
	20.0	2.8	4,627	692	692	3.684	0.129	3.409	0.120
	25.0	2.9	4,585	881	883	5.077	0.154	4.666	0.142
	35.0	2.8	4,731	1,420	1,425	7.393	0.164	7.009	0.157
	40.0	2.9	4,698	1,477	1,477	8.306	0.178	7.805	0.170
14	1.0	6.5	3,950	536	545	18.011	0.723	14.326	0.582
	2.5	4.5	4,136	512	514	7.875	0.325	6.540	0.273
	7.5	3.5	4,518	376	376	3.203	0.158	2.894	0.146
	12.5	3.2	4,568	521	523	3.669	0.151	3.365	0.139
	15.0	3.2	4,608	595	600	4.154	0.159	3.860	0.148
	20.0	3.2	4,666	889	889	6.129	0.185	5.720	0.174
	25.0	3.2	4,701	1,110	1,115	7.596	0.199	7.174	0.189
	30.0	3.2	4,746	1,233	1,236	8.358	0.205	7.948	0.196
	35.0	3.1	4,771	1,535	1,535	9.713	0.206	9.269	0.197
	40.0	3.1	4,821	1,680	1,685	10.521	0.207	10.174	0.202

TABLE II

Trajectory calculations results for the reaction HS(0, 1) + O_2(v″, 1) (continuation).

v″	E_{tr} (Kcal/mol)	b_{max} (Å)	N_T^{IEQMT}	N_r^{IEQMT}	N_r^{QCT}	σ^r_{IEQMT}	$\Delta\sigma^r_{IEQMT}$	σ^r_{QCT}	$\Delta\sigma^r_{QCT}$
27	1.0	6.9	4,475	2,036	2,056	68.051	1.113	61.504	1.041
	2.5	6.3	4,582	1,865	1,873	50.752	0.905	46.709	0.854
	7.5	5.3	4,739	1,630	1,634	30.353	0.609	28.839	0.585
	12.5	4.4	4,891	2,149	2,158	26.723	0.432	26.237	0.426
	15.0	4.2	4,912	2,231	2,245	25.170	0.394	24.852	0.390
	20.0	4.0	4,901	2,302	2,318	23.610	0.358	23.244	0.355
	25.0	3.9	4,902	2,382	2,388	23.219	0.341	22.811	0.338
	30.0	3.8	4,908	2,481	2,507	22.932	0.324	22.673	0.321
	40.0	3.7	4,880	2,579	2,608	22.729	0.307	22.392	0.304

in previous paragraphs, there are only small quantitative differences between IEQMT and QCT results. Thus, the discussion hereafter is valid for both results, even when only the QCT results are being considered.

The curves in Figure 2 have in general two different trends. For internal energies of the excited O_2 molecule below 47.59 kcal/mol ($v'' = 0, 5, 9$) the shape of these curves correspond to a barrier-type behavior for the whole range of translational energies. This case is represented in the inset of the figure. Instead, for larger vibrational energy values ($v'' = 12, 14, 27$ main plot of the figure), the capture-type regime dominates at low translational energies, leading to the well established decreasing of the reactive cross section as E_{tr} is increased. Furthermore, for higher translational energies, one observes a typical pattern for reactions with energy threshold, i.e., an increase in the cross-section at $v'' = 12, 14$. As a result, the excitation function for such cases shows a minimum in the region where the afore mentioned behaviors balance each other.

To analytically describe the dependence of the cross-section on the translational energy, we have used the expression [29]:

$$\sigma^r_{0,v''}(E_{tr}) = \frac{f(v'')}{E_{tr}^{n(v'')}} + g(v'')E_{tr}^{e(v'')} \exp[-d(v'')E_{tr}] \quad (3)$$

for the capture regime, and

$$\sigma^r_{0,v''}(E_{tr}) = g_1(v'')\left[E_{tr} - E^{th}_{tr}(v'')\right]^{e_1(v'')} \times \exp\left\{- d_1(v'')\left[E_{tr} - E^{th}_{tr}(v'')\right]\right\} \quad (4)$$

for the barrier one.

To consider the effect of internal energy we assume a Taylor series expansion up to the second order around $v'' = 12$ of the type $a_0 + a_1(v'' - 12) + a_2(v'' - 12)^2$ for auxiliary functions $f(v'')$, $g(v'')$ and parameters $n(v'')$, $e(v'')$ and $d(v'')$. In a similar form, function $g_1(v'')$ and parameters $E^{th}_{tr}(v'')$, $e_1(v'')$, and $d_1(v'')$ were expanded around $v'' = 0$.

TABLE III

Trajectory calculations results for the combination HS(0, 1) + O_2(27, 1), pure QCT.

E_{tr} (Kcal/mol)	b_{max} (Å)	N_T	HS + O_2	OH + SO	H + SO_2	HSO + O	HO_2 + S	H + O+ SO	OH + S + O	O_2 + S + H	HS+ O + O
1.00	6.9	5,000	2,944	334	469	910	83	238	0	22	0
2.50	6.3	5,000	3,127	265	406	891	119	185	0	7	0
7.50	5.3	5,000	3,366	222	312	819	52	212	2	15	0
12.50	4.4	4,998	2,842	244	344	1,206	59	284	5	14	0
15.00	4.2	4,995	2,755	280	352	1,240	63	275	2	28	0
20.00	4.0	4,989	2,682	229	401	1,309	77	271	6	14	0
25.00	3.9	4,998	2,612	237	372	1,371	32	329	12	31	2
30.00	3.8	4,984	2,493	276	368	1,371	58	373	17	15	13
35.00	3.7	4,981	2,425	279	341	1,467	43	357	22	24	23
40.00	3.7	4,990	2,392	253	320	1,436	47	435	30	27	50

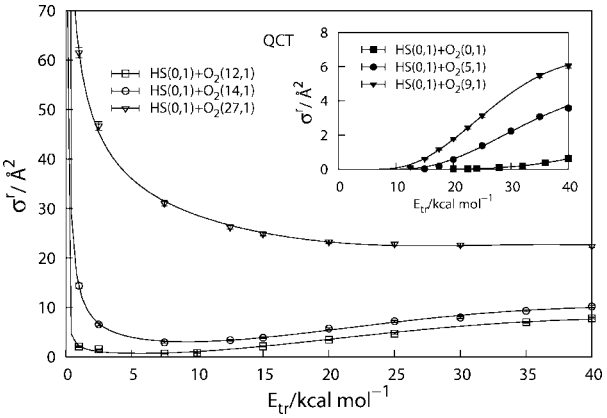

FIGURE 2. Specific total reactive cross section from calculations in this work for pure QCT results. Low vibrational energies of O_2 reactant are displayed in the inset, whereas main plot shows high vibrational energies.

The expansion coefficients for the auxiliary functions and the parameters in Eqs. (3–4) have been determined from two least-squares fitting procedures, one for $v'' \geq 11$ (capture regime) and the other for the remaining combinations of vibrational quantum numbers corresponding to a barrier regime. Their optimum numerical values are reported in Table IV. The resulting fitted functions are shown together with the calculated points in Figure 2. It is seen that the model reflects the general trends of the calculations.

4.3. REACTIVE THERMAL RATE COEFFICIENTS

Substituting Eq. (3) and (4) in Eq. (2) and performing the integration analytically, the specific reactive thermal rate coefficient $k^r_{0,v''}(T)$ assumes the form:

$$k^{\mathrm{r,cap}}_{0,v''}(T) = g_{\mathrm{e}}(T)\left(\frac{8}{\pi\mu}\right)^{1/2}\{f(v'')(k_{\mathrm{B}}T)^{1/2-n(v'')}\Gamma[2-n(v'')] + g(v'')\,\frac{(k_{\mathrm{B}}T)^{\mathrm{e}(v'')+1/2}}{(1+\,d(v'')k_{\mathrm{B}}T)^{\mathrm{e}(\mathrm{v}'')+2}}\,\Gamma[\mathrm{e}(v'')+2]\} \quad (5)$$

$$k^{\mathrm{r},bar}_{0,v''}(T) = g_{\mathrm{e}}(T)\left(\frac{8}{\pi\mu}\right)^{1/2} g_1(v'') \times \frac{(k_{\mathrm{B}}T)^{e_1(v'')+2}}{(1+d_1(v'')k_{\mathrm{B}}T)^{\mathrm{e}_1(v'')+2}}\exp\left(-\frac{E^{\mathrm{th}}_{\mathrm{tr}}}{k_{\mathrm{B}}T}\right)\times \times\left[\Gamma(e_1(v'')+2)+\Gamma(e_1(v'')+1) \times (1+d_1(v'')k_{\mathrm{B}}T)\,\frac{E^{\mathrm{th}}_{\mathrm{tr}}}{k_{\mathrm{B}}T}\right] \quad (6)$$

where Γ is the gamma function. Equation (5) describes the reactive rate coefficients for the capture regime, whereas equation (6) represents the barrier behavior. Figure 3 shows specific rate coefficients obtained from Eqs. (5–6) for vibrational quantum numbers $v'' = 0, 5, 9, 12, 14, 27$ of the O_2 molecule. As expected, two different patterns, corresponding to barrier and capture regimes, are observed. For $v'' \leq 11$ and low temperatures the rate constants have small values, which rapidly increase when temperature is raised. Nevertheless, in such a range of vibrational quantum numbers, the specific rate coefficients get higher values as initial vibrational energy of O_2 is raised. At low temperatures, the rate constant

TABLE IV

Numerical values[a] for coefficients of the cross-section functions.

Functions/	QCT			IEQMT		
parameters	a_0	a_1	a_2	a_0	a_1	a_2
$f(v'')$	2.23051	6.27948	−0.154867	2.66732	6.70279	−0.159487
$g(v'')$	0.00096275	2.96805×10^{-10}	-4.27891×10^{-6}	0.00096275	2.97215×10^{-10}	-4.27891×10^{-6}
$n(v'')$	0.823	-3.07692×10^{-7}	−0.00217785	0.8523	-1.07692×10^{-7}	−0.00217785
$e(v'')$	3.18703	-1.92308×10^{-10}	0.0265369	3.18703	-1.92308×10^{-10}	0.0265369
$d(v'')$	0.0698935	0.000964005	0.000554397	0.0698935	0.000964005	0.000554397
$g_1(v'')$	8.5329×10^{-5}	0.000207465	-1.40222×10^{-5}	0.000233019	0.0244586	−0.00142934
$e_1(v'')$	2.858430	0.0300294	0.00246611	2.43364	−0.347678	0.026755
$d_1(v'')$	0.0080001	0.0159918	−0.000850243	−0.0174557	0.0114093	−0.000682778
$E^{\mathrm{th}}_{\mathrm{tr}}(v'')$	16.063	−1.79066	0.0707916	16.5809	0.240016	−0.0931379

[a] The units are such that cross section in Eqs. (3) and (4) is Å^2 and energy is kcal/mol.

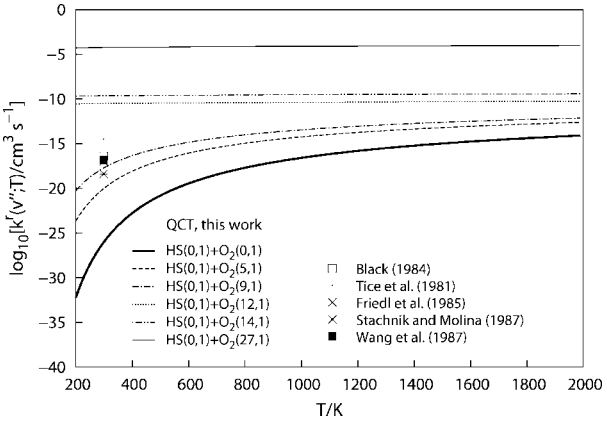

FIGURE 3. Specific reactive thermal rate coefficients for QCT results in this work.

values for the studied vibrational quantum numbers differ from each other up to several orders of magnitude. At higher internal energies of oxygen molecules the specific rate coefficients show small variation through the whole range of reported temperature. For high temperature all curves approach each other with a tendency to a plateau. Figure 3 also displays the experimental rate constant values reported in literature for title reaction [30–34].

For completeness we report vibrationally averaged reactive thermal rate coefficients, obtained as:

$$k^{\mathrm{r}}(T) = \frac{\sum_{v''=0} \omega_{v''} k^{\mathrm{r}}_{0,v''}}{\sum_{v''=0} \omega_{v''}} \tag{7}$$

where $\omega_{v''}$ stands for vibrational states population distribution of the molecular oxygen.

We are also interested in studying reaction (1) in atmospheric conditions. For this purpose we used in Eq. (7) the distribution of vibrational states of O_2 resulting from the photolysis of O_3 at 226 and 266 nm [9]. The photolysis at 226 nm produces relatively large populations of O_2 in highly excited vibrational levels (with a maximum at $v'' = 27$) while at 226 nm the photolysis produces O_2 molecules less vibrationally excited (with maxima near $v = 5$ and $v'' = 9$). The average rate constants obtained with these two distributions are displayed in Figure 4. From this figure it can be seen that the rate constants are very large when compared to the available experimental data at 300 K. However, averaged rate constants in good agreement with the experiments can be obtained if one considers that only the populations from the photolysis at 266 nm up to the level $v'' = 11$ contribute to the summation in Eq. (7). Notice that $v'' = 11$ represents the largest vibration quantum number from the barrier regime observed in the excitation functions in Figure 2. Thus, even the inclusion of low excited vibrational levels of O_2, corresponding to barrier regime, in the excitation functions, produces a significant increase in the rate constant values of the reaction (1).

4.4. COMPARISON BETWEEN HS EXCITED AND O_2 EXCITED CASES

Figure 5 shows a comparison of the total reactive cross-section (5a) and specific reactive thermal rate coefficient (5b) for two sets of reactants with nearly the same internal energy (E_{int}): combinations HS(3, 1) + O_2(0, 1) ($E_{\mathrm{int}} = 27.64$ kcal/mol), HS(0, 1) + O_2(5, 1) ($E_{\mathrm{int}} = 27.62$ kcal/mol), HS(5, 1) + O_2(0, 1) ($E_{\mathrm{int}} = 40.56$ kcal/mol) and HS(0, 1) + O_2(9, 1) ($E_{\mathrm{int}} = 43.76$ kcal/mol). The results indicate that to promote reactions it is more effective to excite the oxygen molecule than the HS radical.

The above statement can be rationalized as follows: adding vibrational energy in O_2 molecule increase the O–O bond distance favoring a direct pathway toward HSO formation. Notice that O–O bond distances in HSOO and HSO···O intermediate structures (see Fig. 1) are larger than the corresponding for the ground vibrational state of O_2 [18]. For these intermediate species, H − S bond distance remain almost the same as for ground state mercapto radical [18]. Hence, vibrational excitation energy in

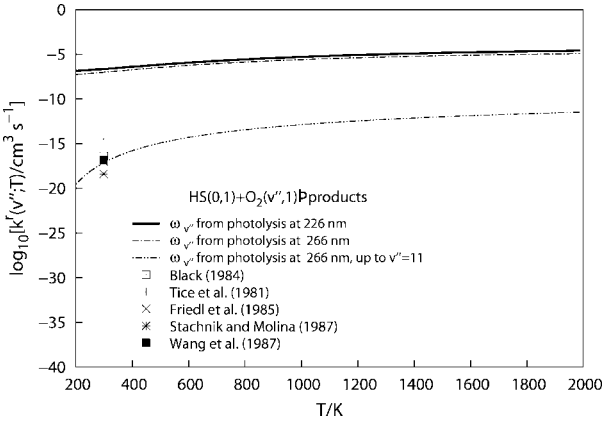

FIGURE 4. Vibrationally averaged reactive thermal rate coefficients. Population distributions for levels of O_2 are from O_3 photodysociation at 226 and 266 nm and from the one at 266 nm, keeping vibrational levels populated only up to $v'' \leq 11$.

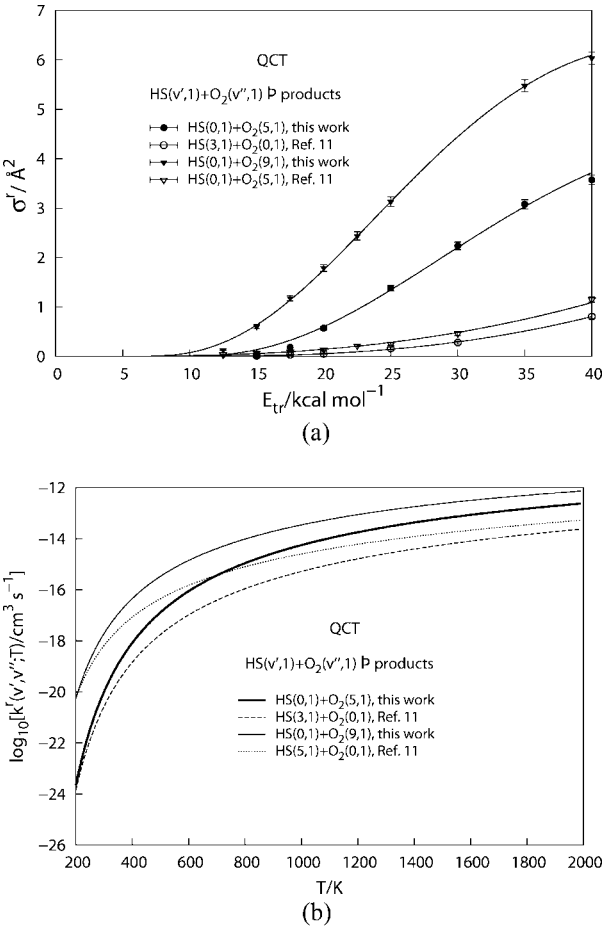

FIGURE 5. Comparison between vibrational excitation effects of HS radical and O_2 molecule. Panel (a) specific total reactive cross section; Panel (b) specific reactive thermal rate coefficients. All results from pure QCT calculations.

HS needs to be transferred to the moiety during the collision, to get products.

Considering that in the atmosphere it is more probable to find vibrationally excited oxygen molecule than excited HS radical, title reaction with an excited O_2 molecule could be more important than reaction

$$HS(v', j' = 1) + O_2(v'' = 0, j'' = 1) \rightarrow \text{products} \quad (8)$$

to explain atmospheric chemical cycles. On the other hand, under typical experimental conditions [30–34], the use of O_2 as vibrational quencher of excited HS radical introduces vibrational–vibrational energy transferences between both molecules producing vibrational excited oxygen and hence the possibility of allowing reaction (1) to occur. This argument also supports the concordance of our calculations with experimental results.

5. Conclusions

A quasiclassical study of the title reaction was reported. Specific calculations at different vibration quantum numbers of O_2 were carried out to assert the role of vibrational excitation of the oxygen molecule. Reactivity increases as vibrational energy gets higher values. Total reactive cross-sections showing two different patterns, barrier and capture, are reported and fitted to models. The vibrational quantum number of O_2, $v'' = 11$ denotes the limit value, for which there is a change in the patterns for excitation functions. Specific rate coefficients are analytically described for a wide range of temperature. To reproduce experimental results vibrational excitation of reactants must be accounted for. There is a general trend to obtain higher reactivity when the internal energy is deposited into O_2 reactant instead than in HS radical. The obtained values for specific rate coefficients are high and then, the inclusion of these reactions in atmospheric models could be necessary.

References

1. Finlayson-Pitts, B. J.; Kleindienst, T. E.; Ezell, M. J.; Toohey, D. W. J Chem Phys 1981, 74, 4533.
2. Ohoyama, H.; Kasai, T.; Yoshimura, Y.; Kuwata, H. Chem Phys Lett 1985, 118, 263.
3. Slanger, T.; Jusinski, L.; Black, G.; Gadd, G. E. Science 1988, 241, 945.
4. Rogaski, C. A.; Price, J. M.; Mack, J. A.; Wodtke, A. M. Geophys Res Lett 1993, 20, 2885.
5. Slanger, T. G. Science 1994, 265, 1817.
6. Summers, M. E.; Conway, R. R.; Siskind, D. E.; Stevens, M. H.; Offermann, D.; Riese, M.; Preusse, P.; Strobel, D. F.; Russell, J. M. Science 1997, 277, 1967.
7. Miller, R. L.; Suits, A. G.; Houston, P. L.; Toumi, R.; Mack, J. A.; Wodke, A. M. Science 1994, 265, 1831.
8. Garrido, J. D.; Caridade, P. J. S. B.; Varandas, A. J. C. J Phys Chem A 2002, 106, 5314.
9. Geiser, J. D.; Dylewski, S. M.; Mueller, J. A.; Wilson, R. J.; Toumi, R.; Houston, P. L. J Chem Phys 2000, 112, 1279.
10. Guerrero, Y. O.; Garrido, J. D. Revista Cubana de Física 2006, 22, 45.

11. Ballester, M. Y.; Guerrero, Y. O.; Garrido, J. D. Int J Quantum Chem 2008, 108, 1705.
12. Finlayson-Pitts, B. J.; Pitts, J. N., Jr. Atmospheric Chemistry; Wiley: New York, 1986.
13. Stranges, D.; Yang, X. M.; Chesko, J. D.; Suits, A. G. J Chem Phys 1995, 102, 6067.
14. Atkinson, R.; Baulch, D. L.; Cox, R. A.; Hampson, R. F., Jr.; Kerr, J. A.; Rossi, M. J.; Troe, J. J Phys Chem Ref Data 1997, 26, 521.
15. Takahashi, K.; Hayashi, S.; Matsumi, Y. N.; H.Taniguchi, S. J Geophys Res 2002, 107, 4440.
16. Varandas, A. J. C.; Wang, W. Chem Phys 1997, 215, 167.
17. Wang, W.; González-Jonte, R.; Varandas, A. J. C. J Phys Chem A 1998, 102, 6935.
18. Ballester, M. Y.; Varandas, A. J. C. Phys Chem Chem Phys 2005, 7, 2305.
19. Ballester, M. Y.; Varandas, A. J. C. Chem Phys Lett 2007, 433, 279.
20. Ballester, M. Y.; Caridade, P. J. S. B.; Varandas, A. J. C. Chem Phys Lett 2007, 439, 301.
21. Ballester, M. Y.; Varandas, A. J. C. Int J Chem Kin 2008, 40, 533.
22. Ballester, M. Y.; Varandas, A. J. C. Int J Chem Kin Ref: KIN-08-0095.R1 (in press).
23. Hase, W. L. MERCURY: A general Monte-Carlo classical trajectory computer program, QCPE#453; An updated version of this code is VENUS96: W. L. Hase, R. J. Duchovic, X. Hu, A. Komornik, K. F. Lim, D.-H. Lu, G. H. Peslherbe, K. N. Swamy, S. R. van de Linde, A. J. C. Varandas, H. Wang, R. J. Wolf, QCPE Bull 1996, 16, 43.
24. Varandas, A.; Pais, A.; Marques, J.; Wang, W. Chem Phys Lett 1996, 249, 264.
25. Karplus, M.; Porter, R.; Sharma, R. D. J Chem Phys 1965, 43, 3259.
26. Truhlar, D. G. J Chem Phys 1972, 56, 3189.
27. Muckerman, J. T.; Newton, M. D. J Chem Phys 1972, 56, 3191.
28. Varandas, A. J. C. Chem Phys Lett 1994, 225, 18.
29. Garrido, J. D.; Caridade, P. J. S. B.; Varandas, A. J. C. J Phys Chem A 1999, 103, 4815.
30. Black, G. J Chem Phys 1984, 80, 1103.
31. Tice, I. J.; Wampler, F. B.; Oldenborg, R. C.; Rice, W. W. Chem Phys Lett 1981, 82, 80.
32. Friedl, R. R.; Brune, W. H.; Anderson, J. G. J Phys Chem 1985, 89, 5505.
33. Stachnick, R. A.; Molina, M. J. J Phys Chem 1987, 91, 4603.
34. Wang, N. S.; Lovejoy, E. R.; Howard, C. J. J Phys Chem 1987, 91, 5743.